Tuning Caco-2 Permeability by Cocrystallization: Insights from Molecular Dynamics Simulation

Noopur Pandey^a, Nimmy Kumari^a, Parag Roy^a, Susanta Kumar Mondal^b, Abhishek Thakur^{c*}, Changquan Calvin Sun^{d*} and Animesh Ghosh^{a*}

^a Solid State Pharmaceutics Research Lab, Department of Pharmaceutical Sciences and Technology, Birla Institute of Technology, Mesra, Ranchi 835215, Jharkhand, India.

^b TCG Life Sciences Pvt. Ltd, Block-EP & GP, BIPL, Tower-B, Salt Lake, Sector-V, Kolkata, 700091, India.

- ^c Department of Chemistry, University of Miami, Coral Gables, Florida 33146, United States
- ^d Pharmaceutical Materials Science and Engineering Laboratory, Department of Pharmaceutics, College of Pharmacy, University of Minnesota, 9-127B Weaver-Densford Hall, 308 Harvard Street S.E., Minneapolis, MN 55455, United States.

*Corresponding Authors:

1. Animesh Ghosh, PhD

Associate Professor

Department of Pharmaceutical Sciences and Technology,

Birla Institute of Technology, Mesra

Ranchi 835215, Jharkhand, India

E-mail: aghosh@bitmesra.ac.in, anim 1607@yahoo.co.in

2. Changquan Calvin Sun, PhD

Professor and Associate Department Head

Department of Pharmaceutics,

College of Pharmacy

University of Minnesota,

9-127B Weaver-Densford Hall, 308 Harvard Street S.E.

Minneapolis, MN 55455, United States

Email: sunx0053@umn.edu

3. Abhishek Thakur, PhD

Department of Chemistry, University of Miami,

Coral Gables, Florida 33146, United States

Email: axt651@miami.edu

Abstract

Emerging evidence suggests that intestinal permeability can be potentially enhanced through cocrystallization. However, a mechanism for this effect remains to be established. In this study, we first demonstrate the enhancement in intestinal permeability, evaluated by the Caco-2 cell permeability assay, of acetazolamide (ACZ) in the presence of a conformer, *p*-aminobenzoic acid (PABA), delivered in the form of a 1:1 cocrystal. The binding strength of ACZ and PABA with the Pgp efflux transporter, either alone or as a mixture, was calculated using molecular dynamics simulation. Results show that PABA weakens the binding of ACZ with Pgp, which leads to a lower efflux ratio and elevated permeability of ACZ. This work provides molecular-level insights into a potentially effective strategy to improve the intestinal permeability of drugs. If the same cocrystal also exhibits higher solubility, oral bioavailability of BCS IV drugs can likely be improved by forming a cocrystal with a Pgp inhibitor.

- 13 Keywords: Cocrystallization, permeability; acetazolamide, Caco-2 cell; P-glycoprotein;
- 14 efflux; all-atom molecular dynamics.

1. Introduction

15

16

17

18

19

20

21

22

23

24

25

26

27

28

29

30

31

32

33

34

35

36

37

38

39

40

41

42

43

44

45

46

47

48

The use of different solid forms, such as salts, cocrystals, hydrates, solvates, and polymorphs, is an effective engineering approach to modulate the physicochemical properties of drugs. Among these, cocrystallization stands out because of its applicability to non-ionizable drugs and the ability to access a wide range of chemical space of cocrystal formers for modifying crystal structure and properties without changing their molecular structures or pharmacological activities (Kumari and Ghosh, 2020; Roy and Ghosh, 2020a; Sun, 2013). Various pharmaceutically important drug properties, such as solubility (Kumari et al., 2019; Kundu et al., 2018; Roy et al., 2022; Roy and Ghosh, 2020b; Sugandha et al., 2014), permeability (Bommaka et al., 2018; Mannava et al., 2023, 2021; Palanisamy et al., 2021; Sanphui et al., 2015; Shajan et al., 2023), tabletability (Kavanagh et al., 2021; Kumari et al., n.d.; Sun and Hou, 2008; J. Wang et al., 2021; X. Wang et al., 2021; Zhou et al., 2016), stability (Hao et al., 2022; Vangala et al., 2012), hygroscopicity (Shinozaki et al., 2019; Tanaka et al., 2020), and oral bioavailability (Chen et al., 2022; Wang et al., 2022), have been extensively studied to demonstrate the potential of cocrystallization in pharmaceutical formulation and drug delivery. Orally administered drugs must have adequate oral bioavailability in order to be therapeutically effective. Both dissolution and permeability of drugs play a key role in attaining adequate bioavailability (U.S. Department of Health and Human Services et al., 2008). Despite a large number of publications focusing on the solubility and dissolution enhancement of drugs through cocrystallization (Ahangar et al., 2023; Kataoka et al., 2023), the exploration of modulating drug intestinal permeability by cocrystallization has received little attention. With a few exceptions, papers on the topic of drug permeability modification by cocrystallization mostly demonstrated an improvement in flux of drug across a membrane, instead of permeability. For example, a recent study showed a permeability improvement of 9.69-fold by a salt cocrystal over the parent drug, milrinone (Meng et al., 2023). While there is a growing body of evidence that suggests the possibility for modulating intestinal permeability through cocrystallization, a mechanistic explanation is lacking. Since dissolved drug molecules have no memories of their solid-state predecessor, modifications of drug permeability must involve the coformer. A mechanistic understanding of any observed intestinal permeability enhancement by cocrystals will be extremely useful for developing guidelines for designing cocrystals with improved bioavailability (Bommaka et al., 2018; Mannava et al., 2021; Palanisamy et al., 2021; Sanphui et al., 2015).

Recently, three potential factors that can lead to the permeability modulation of a drug through cocrystallization were proposed: (i) drug-coformer intermolecular interactions and

structure-permeability correlation, (ii) solubility-dependent concentration gradient, and (iii) coformer induced lipophilicity and diminished molecular polarity (Pandey and Ghosh, 2022). These factors pertain to passive diffusion of drugs through membrane and their role in bioavailability enhancement still need to be experimentally established. Some issues that need to be addressed when studying the permeability of cocrystals include 1) distinction of flux from permeability, 2) consideration of the dissociation of drug-coformer complexes in solution media, and 3) measuring permeability under conditions resembling the real intestinal membrane where majority of absorption takes place (Diniz et al., 2020; Li et al., 2021; Seo et al., 2018; Suzuki et al., 2019). The dissociation of drug-coformer complexes upon dissolution of a cocrystal means the permeability modulation cannot be explained by the drug-coformer intermolecular interactions observed in cocrystals. Compared to polymeric membranes used for permeability using the Franz diffusion cell (FDC) (Ng et al., 2010), Caco-2 cell membranes more accurately simulate in vivo conditions in terms of both active and passive diffusion as well as the expression of efflux transporters. P-glycoprotein (Pgp), an ATP-dependent efflux pump, is a transmembrane protein expressed in the intestinal membrane, blood-brain barrier, liver, and kidneys (Varma et al., 2005). Pgp has the ability to "pump out" drugs from cells, making it a significant barrier to absorption and, thereby, oral bioavailability, of drugs that are Pgp substrates (Amin, 2013; El-Awady et al., 2017). Therefore, measuring permeability through a Caco-2 cell monolayer is more advantageous for understanding the effects of cocrystallization on intestinal permeability.

All-atom molecular dynamics (MD) simulations in the apo and halo states can potentially provide insights into how the presence of coformer molecules affects the interactions between drug molecules and a receptor, such as Pgp. This is achieved by comparing relative binding affinity of Pgp-drug complexes with and without the presence of coformer. Weakening of drug binding to Pgp by coformer molecules, e.g., competitively, non-competitively, or allosterically (Amin, 2013), leads to less effective removal of the drug by Pgp (Seelig, 2020), which leads to enhanced intestinal permeability. If proven useful, the MD approach can be used to virtually select coformers capable of enhancing the intestinal permeability of drugs for more effective therapies through crystal engineering.

In this work, we investigated the effects of cocrystallization on permeability of acetazolamide (ACZ), using a 1:1 cocrystal with *p*-aminobenzoic acid (PABA). ACZ is a Biopharmaceutics Classification System (BCS) class IV drug with low solubility and low permeability (Ghadi and Dand, 2017).

2. Material and Methods

2.1 Materials

Pure ACZ was obtained as a gift from Nakoda Chemicals Ltd. (Hyderabad, India). PABA was purchased from Sigma-Aldrich (St. Louis, Missouri, United States). All other inactive ingredients were of pharmaceutical grade. Solvents were purchased from Rankem (Gurgaon, Haryana). All analytical chemicals and solvents were used as received without further purification. Scheme 1 illustrates the chemical structures of ACZ and PABA.

HO NH_2 (B)

Scheme 1: Chemical structures of (A) Acetazolamide and (B) *p*-aminobenzoic acid.

2.2.1. Preparation of cocrystal

In this study, we prepared an ACZ-PABA cocrystal, equivalent to 500 mg ACZ, using a slurry technique. Here, 2.2 mmol of ACZ and 2.2 mmol of PABA were added to 2 mL of ethyl alcohol in a beaker, which was then sealed with parafilm. The slurry was stirred at room temperature for 24 hours, filtered, and dried at 50°C. We also determined the crystal structure of ACZ-PABA cocrystal (CCDC NO: 1984314), which is in agreement with that reported by Manin et.al. (CCDC NO. 1999205) (Manin et al., 2020). The detailed crystallographic methodology and crystal structural information (Table S1, Figure S1) can be found in the supporting information.

2.2.2. Powder X-Ray diffraction (PXRD)

PXRD data was collected using a Rigaku smart lab diffractometer (Model Miniflex 600; Rigaku, Tokyo, Japan) with Cu K α radiation (λ = 1.5406 Å) at 40 kV (tube voltage) and 1 mA (tube current). Samples were placed on a sample holder and slightly compressed with a glass slide to ensure coplanarity of the sample surface with sample holder surface. X-ray patterns were recorded over a 20 range of 3° to 40° with a step size of 0.02° at a rate of 10°/min. The PXRD of ACZ-PABA cocrystal was also calculated from its crystal structured (CCDC No. 1999205) (Manin et al., 2020).

2.2.3. Thermal analyses

A differential scanning calorimeter (DSC-4000, PerkinElmer, USA) was used for DSC analysis. Samples were hermetically sealed in aluminum pans and scanned over a range of 30 to 300 °C at a heating rate of 10 °C/min under a dry nitrogen purge (20 mL/min). For TGA analysis, samples were kept in ceramic crucibles and scanned on a TGA-4000 (PerkinElmer, USA) over a range of 30 to 400 °C at 10 °C/min under continuous nitrogen gas purge (20 mL/min).

2.2.4. Dissolution

Dissolution rate is more informative over equilibrium solubility for predicting bioavailability, especially for materials that undergo dissociation, such as cocrystal (Babu and Nangia, 2011). Therefore, powder dissolution and intrinsic dissolution studies were carried out for both the cocrystal and ACZ. As the solubility of ACZ-PABA cocrystal is independent of pH in the physiologically relevant pH range, both powder and intrinsic dissolution experiments were performed in 900 mL of 0.01N hydrochloric acid medium at 100 rpm, 37 ± 0.5 °C, as prescribed by the U.S. Pharmacopoeia (Arenas-García et al., 2017).

2.2.4.1. High performance liquid chromatography (HPLC) operating conditions

The concentrations of ACZ in the solutions from dissolution studies were measured using an HPLC system (Thermo Fisher Scientific, UltiMate 3000) equipped with a photodiode array (PDA) detector. The HPLC system was controlled with workstation software Chromeleon 7 (version 7.2.10). A Syncronis C_{18} column (250 mm × 4.6 mm ID, 5µm particle size, Thermo Scientific, India) was used. The chromatographic separation was achieved using a gradient method using acetonitrile (solvent A) and 0.1% (v/v) orthophosphoric acid (solvent B) in the (v/v) ratio ranging from 80:20 to 85:15. The injection volume was 20 µL and total run time was 12 min. A calibration curve was prepared in the linearity range of 2-16 µg/mL and the absorbance of the eluents was monitored at a detection wavelength of 266 nm. Diluent used for sample preparation was acetonitrile and 0.1% (v/v) orthophosphoric acid in 85:15 (v/v) ratio.

2.2.4.2. Powder dissolution

During in vitro powder dissolution study, ~ 250 mg equivalent ACZ and ACZ-PABA cocrystal were placed in 900 mL of 0.01 N HCl. Aliquots of 2 mL volume were withdrawn at specific time intervals, filtered through a 0.45 μ m nylon membrane, and analysed by HPLC after proper dilution to attain a concentration within that of the predetermined calibration curve.

2.2.4.3. Intrinsic dissolution

For the IDR experiment, ACZ (250 mg) or ACZ-PABA (equivalent to 250 mg of ACZ) was compressed to a disc using a hydraulic press at a pressure of 2.5 tons per square inch for 5

min. Aliquots (1 mL) were withdrawn at specified time intervals of 1, 2, 3, 4, 5, 10, 20, 30, 45, and 60 min, filtered through a $0.45~\mu m$ nylon membrane, and analyzed by HPLC following the same approach as that for powder dissolution.

2.2.5. Caco-2 cell line permeability study

The Caco-2 cell monolayer model was selected in the present investigation to assess the intestinal permeability of ACZ at pH 7.4. Following the standard procedure, Caco-2 cells were cultured in Dulbecco's Modified Eagle Medium (DMEM), containing 10% fetal bovine serum and antibiotics. All cells used in this study were between passages 38 and 50. Cells were plated in 96-well inserts (Corning, Sigma Aldrich, USA) and cultured for 21 days to reach confluence and cell differentiation. Initially, each insert containing the differentiated monolayers was carefully washed and filled with Hank's Balanced Salt Solution (HBSS with 10 mM HEPES, pH 7.4). The integrity of the monolayer was examined using Lucifer Yellow (LY) rejection assay. Wells with less than 1% fluorescence intensity in relation to the Lucifer yellow dosing solution were deemed satisfactory for conducting permeability experiment, which was carried out in both the apical to basolateral $(A \rightarrow B)$ and basolateral to apical $(B \rightarrow A)$ directions. A sample corresponding to 5 µM of ACZ was introduced to the donor side and the system was maintained at 37 °C for 2.5 h without shaking under 5% CO₂ and 95% relative humanity. Samples were collected from both the receiver and the donor compartments, diluted properly, and analyzed using LC-MS/MS (ABSciex API4000 triple quadrupole mass spectrometer, integrated to Prominense LC-20AD series (Shimadzu) LC system & CTC-PAL autosampler, USA).

2.2.6. Molecular docking

Molecular docking is one of the widely adopted methods to predict the binding pose of small molecules (ACZ and PABA here). In this study the 3D structures of ACZ and PABA, acting as ligands, were imported into AutodockTools (Morris et al., 2009), along with the target protein Pgp (PDB ID: 3G5U) (Aller et al., 2009) for molecular docking. According to the established protocol, pre-processing steps, such as adding polar hydrogens, calculating charges, and determining torsions, were taken (Morris et al., 2008; Thakur et al., 2022). The Kollman charges were calculated, and the atomic radii and AutoDock4 atom types were assigned. An exhaustiveness value of 20 was used. The grid size was selected to encompass the complete active site, with a spacing of 1.00 Å. For reference, all docked structures are provided in the supporting information (Figure S2).

2.2.7. Molecular dynamics simulation

The complexes of Pgp protein with ACZ, PABA, and (ACZ + PABA) were subjected to molecular dynamics (MD) simulations. The enzyme complexes were solvated explicitly using an orthorhombic water box (TIP3P), extending 10 Å from the protein (Jorgensen et al., 1983). The system's overall charge was neutralized by adding counter ions as required. The inhibitor was parameterized using the generalized Amber force field (GAFF2) (Vassetti et al., 2019), while the protein topology file was generated using the ff14SB force field (Maier et al., 2015). The MD simulations were performed using the GPU-enabled Amber18 pmemd engine.

The simulation protocol included the initial minimization of water molecules and Na⁺ ions through the conjugate gradient (CG) method for 3,000 followed by 10,000 steps of minimization of the entire complex (protein, ligand, water, and ions), respectively, to achieve system stability. Subsequently, the system was gradually heated from 0 to 300 K over 50 ps using a constant NVT ensemble with a Berendsen thermostat and a temperature coupling value of 2.8 ps. To ensure the desired density, a 500 ps NPT ensemble simulation at 300 K and 1 atm, with temperature and pressure coupling values set to 2.0 ps, was performed. The system was then switched back to the NVT ensemble and equilibrated for an additional 500 ps. Following the minimization and equilibration phase, a 300 ns NVT production run was conducted (Badavath et al., 2022). Long-range electrostatics were accounted for using the particle mesh Ewald method, covalent bonds involving hydrogen atoms were constrained using the SHAKE algorithm, periodic boundary conditions were applied with a non-bonded cutoff distance of 12 Å, and a time step of 1.0 fs was utilized. Analysis of the simulations was performed using cpptraj and ptraj programs from the AmberTools18 suite (Price et al., 2021; Roe and Cheatham, 2018).

The MM/PBSA (Molecular Mechanics/Poisson–Boltzmann Surface Area) methodology was originally developed Kollman and coworkers (Genheden and Ryde, 2015). Subsequent developmental efforts significantly enhanced this approach, making it a crucial tool for investigating ligand binding in diverse biological systems (Shaikh et al., 2015; Wang et al., 2019). It is recognized as a reliable method in estimating the binding free energy of small molecules (Mohd Siddique et al., 2021), or peptides (Cáceres et al., 2018), identifying chirality (Nath et al., 2018), and even guiding target identification (Gangireddy et al., 2022). In this work, the binding affinity of ACZ and PABA was calculated using the MM/PBSA approach available within the Amber package.

3. Results and Discussion

The powder X-ray diffraction (PXRD) pattern of the solid obtained from the ethyl alcohol slurry after 24 hours showed a good agreement with the PXRD pattern simulated from the single-crystal of the ACZ-PABA cocrystal (Figure 1A) (Manin et al., 2020). The formation of a 1:1 ACZ-PABA cocrystal is also supported by thermal analysis. The DSC curves (Figure 1B) showed a distinctive endotherm (217 °C) for the new solid, which lies in between those of ACZ (268 °C) and PABA (190 °C), supporting the formation of a new crystalline phase. The melting temperatures of ACZ and PABA in this study are in good agreement with those reported in the literature (Manin et al., 2020). Further, the TGA curves (Figure 1C) of ACZ, PABA, and the new solid ACZ-PABA cocrystal show no weight loss until melting, indicating thermal stability of these compounds before their respective melting temperatures.

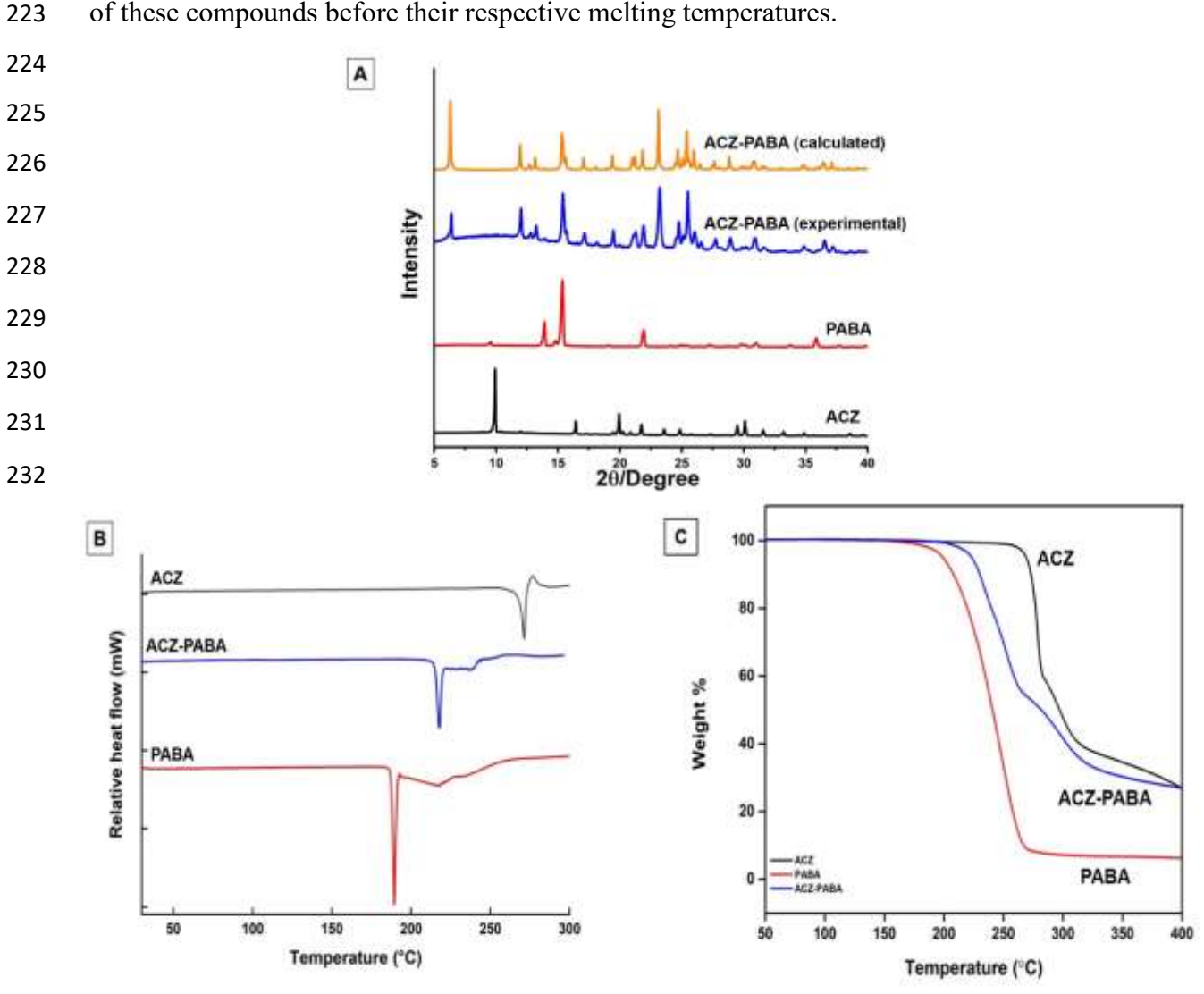


Figure 1. Solid-state characterization of Acetazolamide (ACZ), p-aminobenzoic acid (PABA), and ACZ-PABA. **A)** experimental PXRD patterns along with the pattern calculated from the ACZ-PABA crystal structure, **B)** DSC thermograms, and **C)** TGA thermograms.

The time taken to release half of the total drug dose ($t_{0.5}$) from ACZ-PABA cocrystal (~ 5 min) during powder dissolution (Figure 2A) is approximately one-third of pure ACZ (~ 15 min). The improved dissolution profile of ACZ-PABA cocrystal over ACZ corroborates with the higher aqueous solubility of ACZ-PABA than ACZ. There was no measurable change in solution pH at the end of the powder dissolution experiments.

The IDR of ACZ from ACZ-PABA (0.38 mg cm⁻² min⁻¹) is approximately 1.7 times that of pure ACZ (0.22 mg cm⁻² min⁻¹) (Figure 2B). The IDR ratio is comparable to that of the ratio in apparent solubility (Kumari et al., 2019). Thus, the higher solubility of the ACZ-PABA cocrystal leads to faster dissolution, as expected. This should favor passive diffusion of ACZ through cell membrane, driven by a higher concentration gradient.

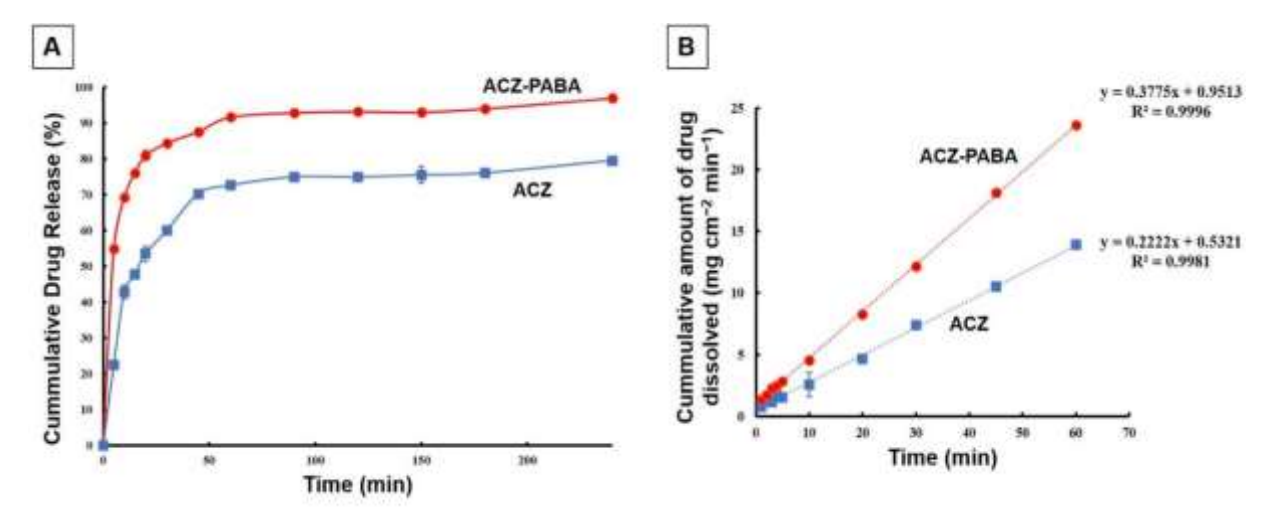


Figure 2. Dissolution profiles of ACZ (square, blue) and ACZ-PABA cocrystal (red, circle) (A) Powder dissolution; (B) Intrinsic dissolution.

The Caco-2 cell lines apparent permeability coefficient (P_{app}) of both apical to basolateral transport $(A \rightarrow B)$ and basolateral to apical transport $(B \rightarrow A)$ and efflux ratios (R) of ACZ, PABA, and ACZ-PABA cocrystal are summarized in Table 1 and graphically shown in Figure 3.

Table 1. Caco-2 cell permeability of ACZ, PABA, and ACZ-PABA cocrystal.

System	<i>P</i> _{app} (×10	R ^c	
	A→B ^a	$B \rightarrow A^b$	IX.
ACZ	0.85 ± 0.05	7.30 ± 1.00	8.59 ± 1.69
PABA	0.35 ± 0.05	1.00 ± 0.00	2.86 ± 0.42
ACZ-PABA	1.35 ± 0.05	6.75 ± 0.15	5.00 ± 0.29

 $[\]overline{{}^a}$ Apical to basolateral transport, b Basolateral to apical transport, c efflux ratio = P_{app} ($B \rightarrow A$)/ P_{app} ($A \rightarrow B$)

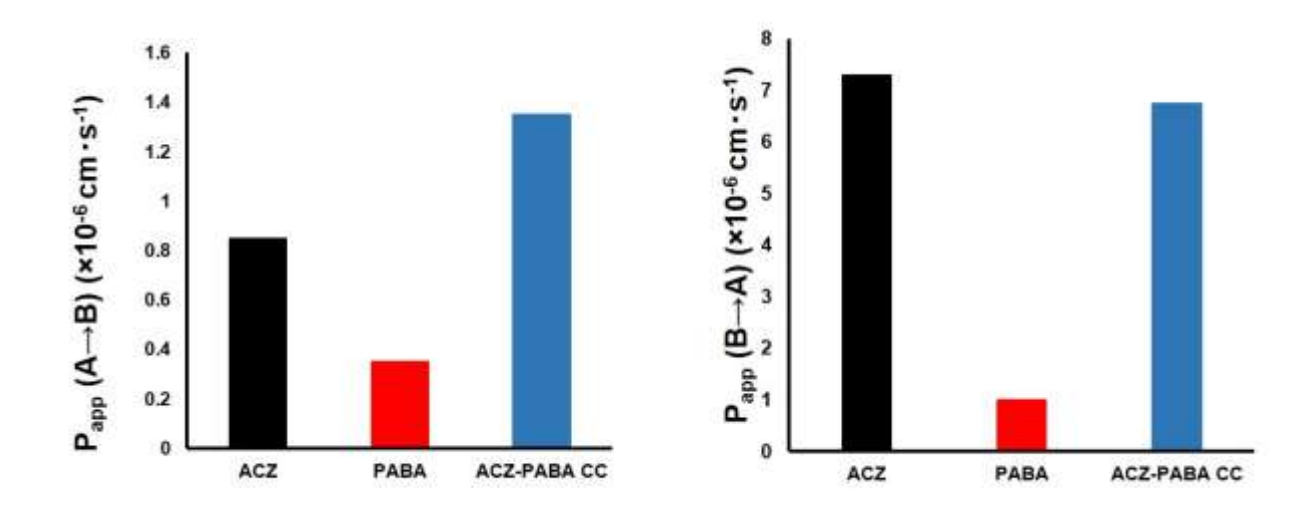


Figure 1. Caco-2 cell permeability ACZ, PABA, and ACZ-PABA cocrystal.

Pgp is further explored by MD simulation.

The comparison of the permeability values of ACZ, PABA, and ACZ-PABA showed that $P_{app}(A\rightarrow B)$ of ACZ-PABA was approximately 59% higher than ACZ (Table 1 and Figure 3). The $P_{app}(B\rightarrow A)$ of ACZ-PABA is 11 % less than the pure ACZ. Consequently, the efflux ratio of ACZ-PABA cocrystal is lower than ACZ. The lower $P_{app}(B\rightarrow A)$ of ACZ-PABA excludes the possibility that a higher concentration gradient of the cocrystal is the dominating driving factor for ACZ to cross the cell membrane. Thus, the higher $P_{app}(A\rightarrow B)$ of ACZ-PABA should not be attributed to the higher solubility and dissolution rate of the cocrystal (Figure 2). However, the different P_{app} can be explained if 1) ACZ is a substrate of the Pgp efflux pump and 2) PABA inhibits the Pgp. This mechanism of competitive binding of ACZ and PABA to

The MM/PBSA method, which combines molecular mechanics energies with Poisson-Boltzmann surface area continuum solvation, was employed to calculate the binding free energy of ACZ and PABA when they are bound to the Pgp receptor. This estimation was carried out over 300 ns MD trajectory, for ACZ and PABA individually, as well as in the presence of each other. The results of the study show that the binding of ACZ to the receptor Pgp is \sim 2 kcal/mol more favorable than the PABA (Table 2). An analysis of the individual energy contributions to the overall binding affinity shows that the van der Waals energy contribution ($E_{\rm vdW}$) and the non-polar solvation-free energy contribution ($E_{\rm rd}$) approximately cancel each other (Table 2). However, the electrostatic energy contribution ($E_{\rm el}$) for ACZ binding (-37.3 kcal/mol) surpasses that of PABA (-12.1 kcal/mol) by more than 3-fold, suggesting that the stronger electrostatic interaction is a primary factor favoring the binding of

ACZ to Pgp. In the presence of PABA, the binding affinity of ACZ to Pgp was reduced by ~ 2 kcal/mol. This effect is expected to slow the efflux process of ACZ by Pgp, which leads to a lower $P_{\text{app}}(B\rightarrow A)$ and higher $P_{\text{app}}(A\rightarrow B)$. This is consistent with the experimental results summarized in Table 1.

Table 2. Calculated binding free energy (in kcal/mol) for ACZ and PABA bound to Pgp receptor over 300 ns of trajectory obtained from MD simulations over four complexes (ACZ-Pgp, PABA-Pgp, ACZ-PABA bound Pgp and PABA-ACZ bound Pgp).

System	${}^*\!E_{ m vdW}$	${}^*\!E$ el	${}^{ullet}G_{ m pol}$	${}^*G_{np}$	$^*\!\Delta G$ bind
ACZ	-23.7 ± 2.1	-37.3 ± 8.6	52.6 ± 6.9	-2.7 ± 0.06	-11.1 ± 3.4
PABA	-21.7 ± 2.3	-12.1 ± 4.2	26.5 ± 4.3	$\textbf{-}2.0 \pm 0.08$	-9.3 ± 2.9
ACZ in presence of	-16.3 ± 3.2	-31.4 ± 10.4	40.4 ± 9.7	$\textbf{-1.8} \pm 0.2$	-9.2 ± 4.5
PABA					
PABA in presence	-18.9± 2.1	-9.71 ± 6.8	21.4 ± 4.6	$\textbf{-2.1} \pm 0.1$	-9.3 ± 2.9
of ACZ					

^{*} $E_{vdW} = van der Waals energy$, $E_{el} = electrostatic energy$, G_{pol} and $G_{np} = polar$ and nonpolar contributions to the solvation free energies, respectively.

To further elucidate the favorable binding of ACZ to Pgp than PABA, Root-mean-square deviations (RMSDs) and root-mean-square fluctuations (RMSFs) of the backbone protein atoms were computed over the 300 ns trajectory for the various Pgp complexes. The analysis of RMSD enables us to understand the timescale required for the stabilization of the protein structure following the binding of ACZ or PABA. The results show that the Pgp protein quickly stabilizes (~20 ns) upon binding with ACZ, whereas both PABA and the (ACZ + PABA) complex take more than 150 ns to reach equilibrium (Figure 4). This faster stabilization of the ACZ-Pgp complex is consistent with its stronger binding affinity.

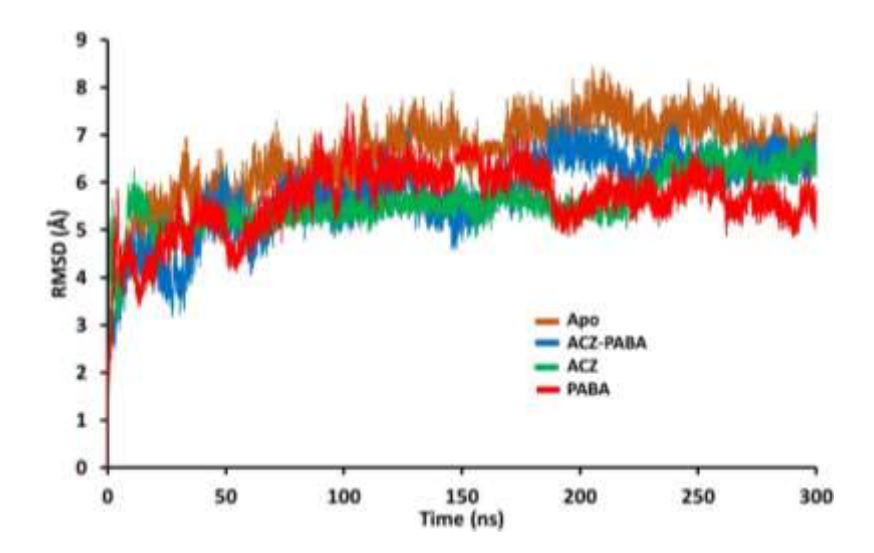


Figure 4. Root-mean-square deviation (RMSD) of the protein backbone atoms (N, $C\alpha$ and C) for the Apo (brown) and holo states of Pgp protein bound to ACZ (green), PABA (red) and (ACZ + PABA) (blue) simulations relative to the first frame.

The impact of ligand binding on protein dynamics can be investigated by analyzing the RMSF of positional changes over time compared to a reference structure. RMSF analysis of the Pgp protein does not show a significant difference in the pattern of fluctuation in response to ligand binding. However, smaller deviations from the reference structure have been observed on average for the Pgp + ACZ complex (Figure 5). We have computed the % change in the RMSF between different substrates bound to the Pgp receptor with respect to the Apo system, where binding of ACZ, PABA, or (ACZ + PABA) complex can cause residues to become more localized (positive change in the % change RMSF) or more flexible (negative change in the % change RMSF). Interestingly, the binding of ligands has shown to have a strong localized effect on protein. However, the binding of ACZ shows the highest % change in RMSF or is more localized in comparison to the binding of PABA, specifically in two regions (residues: 333-350 and 800-880) that encompass the ligand binding site (Figure 6). The RMSD and RMSF analysis results collectively suggest an induced-fit mechanism for both ACZ and PABA. However, overall binding for ACZ is more stable and localized than PABA.

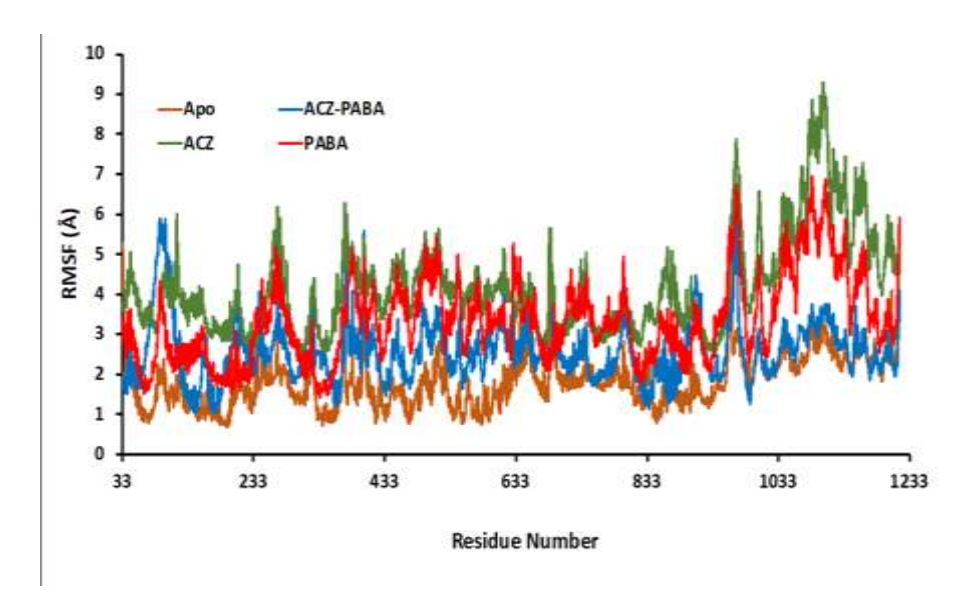


Figure 5. Root-mean-square fluctuations (RMSFs) by residue relative to the average energy structure for the Pgp protein backbone atoms (C, $C\alpha$, and N) in Apo (brown) state and holo state bound with ACZ (green), PABA (red) and (ACZ + PABA) (blue).

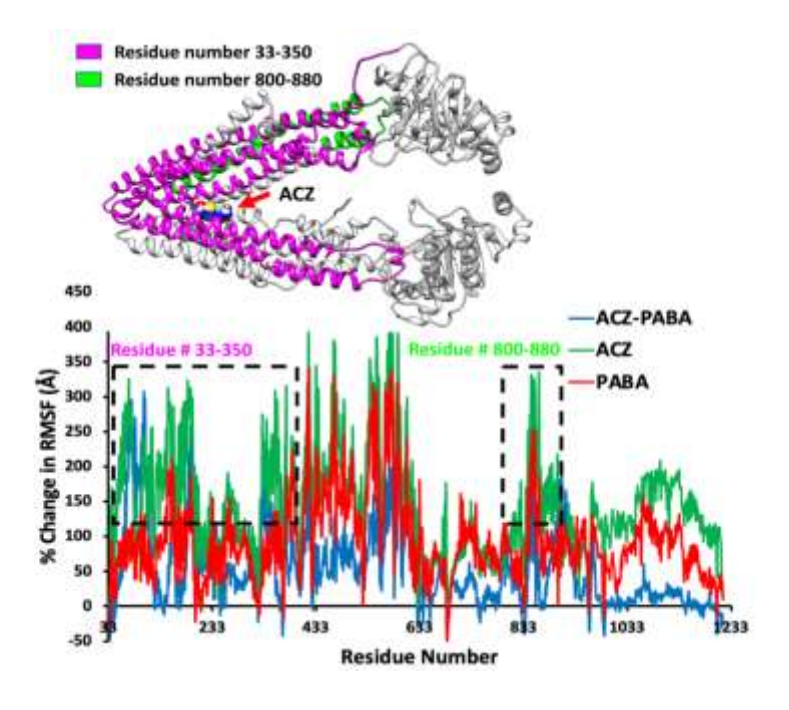


Figure 2. Illustrating the average percent change in root-mean-square fluctuations (RMSF) Pgp receptor backbone atoms (N, Cα and C) upon binding with ACZ (green), PABA (red), and (ACZ + PABA) (blue). A positive change in RMSF shows that residues have become more localized and a negative change is indicative of enhanced fluctuations upon aptamer binding.

In order to understand the strong electrostatic energy ($E_{\rm el}$) contribution of ACZ binding to Pgp receptor, hydrogen bond analysis was carried out. Favorable electrostatic interaction between ACZ or PABA with Pgp was monitored over an entire trajectory and compared with

(ACZ+PABA) complex bound with Pgp. A very strong hydrogen bond between ACZ and G342 was observed, with a population of ~57%. However, this hydrogen bond was completely lost in the (ACZ+PABA) complex. Additionally, a weak hydrogen bond between ACZ and Q343 was reduced from ~21% to 4% in the (ACZ+PABA) complex (Table 3). These results suggest that the presence of PABA disrupts the favorable electrostatic interactions between ACZ and Pgp. Hence, an inhibitory effect by PABA on the efflux process of ACZ is observed.

Table 3. Hydrogen bonds formed between ACZ or PABA and the Pgp receptor over 300 ns of trajectory in three scenarios.

Substrates	Acceptor	Donor	%Occupancy	Length	Angle
ACZ-	E180@OE(1+2)	ACZ@N1H1	25.4	2.7	158.6
PABA	ACZ@OH	D993@NH	6.7	2.9	155.5
	ACZ@O3	F990@NH	5.8	2.9	160
	ACZ@O3	S876 @OGH	5.5	2.8	161.9
	ACZ@O1	Q878 @NEH	5.1	2.9	161
	N347@OD1	ACZN4H	5.0	2.8	161.9
	Q343@OE1	ACZ@N1H	4.1	2.8	158.5
	D184@OD(1+2)	ACZ@N1H	6.6	2.8	155.2
	N717@OD(1+2)	PABA@O2H	15.9	2.7	160.3
	Q721@O	PABA@O2H	11.0	2.7	155.1
ACZ	G342@O	ACZ@N1H	56.9	2.8	163.2
	Q343@OE1	ACZ@N4H	20.8	2.8	159.3
PABA	S989@OG	PABA@N1H	20.9	2.9	154.2
	Q1910E1	PABA@O2H	9.8	2.7	161.9
	S988@O	PABA@N1H	9.3	2.8	157

4. Conclusion

Molecular insights into the enhancing intestinal permeability of ACZ by cocrystallization with PABA were attained in this work by molecular dynamics simulations. Our results show that, for the first time, the presence of PABA weakens the ACZ-Pgp complex stability and, hence, the effectiveness of the efflux process. Consequently, co-delivery of PABA in the form of an ACZ-PABA cocrystal leads to a lower $P_{app}(B\rightarrow A)$, a higher $P_{app}(A\rightarrow B)$, and a lower efflux ratio. This work suggests a mechanism for permeability

- enhancement of drugs by cocrystallizing with a coformer capable of inhibiting their efflux
- process regulated by the Pgp transporter.

354

361

- 355 Credit authorship contribution statement
- 356 Noopur Pandey: Investigation, Data curation, Formal analysis, Writing- original draft.
- Nimmy Kumari: Data curation, Writing review & editing. Parag Roy: Writing review &
- editing. Susanta Kumar Mondal: Data curation. Abhishek Thakur: Data curation, Writing-
- original draft. Changquan Calvin Sun: Conceptualization, Writing review & editing.
- 360 Animesh Ghosh: Conceptualization, Supervision.
 - **Declaration of Competing Interest**
- The authors declare no competing financial interest.
- 363 Acknowledgments
- The authors are thankful to Nakoda Chemicals Ltd. (Hyderabad, India) for providing the gift
- sample of ACZ. The authors sincerely acknowledge the Department of Pharmaceutical
- 366 Sciences and Technology and Central Instrumentation Facility of BIT Mesra, Ranchi for
- providing all the necessary facilities. NP acknowledges the financial support provided in the
- 368 form of an Institute Research Fellowship by BIT Mesra. CCS thanks the National Science
- Foundation for support through the Industry-University Collaborative Research Center grant
- 370 IIP-2137264, Center for Integrated Materials Science and Engineering of Pharmaceutical
- 371 Products (CIMSEPP).

372

373

- References
- 374 Ahangar, A.A., Qadri, H., Malik, A.A., Mir, M.A., Shah, A.H., Dar, A.A., 2023.
- Physicochemical and Anti-fungal Studies of the Pharmaceutical Co-crystal/Salt of
- 376 Fluconazole. Mol Pharm 20, 3471–3483.
- https://doi.org/10.1021/acs.molpharmaceut.3c00087
- Aller, S.G., Yu, J., Ward, A., Weng, Y., Chittaboina, S., Zhuo, R., Harrell, P.M., Trinh, Y.T.,
- Zhang, Q., Urbatsch, I.L., Chang, G., 2009. Structure of P-Glycoprotein Reveals a
- Molecular Basis for Poly-Specific Drug Binding. Science (1979) 323, 1718–1722.
- 381 https://doi.org/10.1126/science.1168750
- Amin, Md.L., 2013. P-glycoprotein Inhibition for Optimal Drug Delivery. Drug Target Insights
- 7, DTI.S12519. https://doi.org/10.4137/DTI.S12519
- Arenas-García, J.I., Herrera-Ruiz, D., Morales-Rojas, H., Höpfl, H., 2017. Interrelation of the
- dissolution behavior and solid-state features of acetazolamide cocrystals. European

- Journal of Pharmaceutical Sciences 96, 299–308.
- 387 https://doi.org/10.1016/j.ejps.2016.09.025
- Babu, N.J., Nangia, A., 2011. Solubility Advantage of Amorphous Drugs and Pharmaceutical Cocrystals. Cryst Growth Des 11, 2662–2679. https://doi.org/10.1021/cg200492w
- Badavath, V.N., Thakur, A., Shilkar, D., Nath, C., Acevedo, O., Ucar, G., Jayaprakash, V.,
- 391 2022. Brain permeable curcumin-based pyrazoline analogs: MAO inhibitory and
- antioxidant activity. J Mol Struct 1268, 133681.
- 393 https://doi.org/10.1016/j.molstruc.2022.133681
- Bommaka, M.K., Mannava, M.K.C., Suresh, K., Gunnam, A., Nangia, A., 2018. Entacapone:
- 395 Improving Aqueous Solubility, Diffusion Permeability, and Cocrystal Stability with
- Theophylline. Cryst Growth Des 18, 6061–6069.
- 397 https://doi.org/10.1021/acs.cgd.8b00921
- Cáceres, T.B., Thakur, A., Price, O.M., Ippolito, N., Li, J., Qu, J., Acevedo, O., Hevel, J.M.,
- 399 2018. Phe71 in Type III Trypanosomal Protein Arginine Methyltransferase 7 (TbPRMT7)
- 400 Restricts the Enzyme to Monomethylation. Biochemistry 57, 1349–1359.
- 401 https://doi.org/10.1021/acs.biochem.7b01265
- Chen, D., Huang, W., Zhang, Q., Zhang, Z., Guo, Y., Vreeman, G., Sun, C.C., Hawley, M.,
- 403 Yang, B.-S., He, X., 2022. Bioavailability-Enhancing Cocrystals: Screening, In Vivo
- 404 Predictive Dissolution, and Supersaturation Maintenance. Cryst Growth Des 22, 5154–
- 405 5167. https://doi.org/10.1021/acs.cgd.1c00950
- 406 Diniz, L.F., Carvalho, P.S., Pena, S.A.C., Gonçalves, J.E., Souza, M.A.C., de Souza Filho,
- J.D., Bomfim Filho, L.F.O., Franco, C.H.J., Diniz, R., Fernandes, C., 2020. Enhancing
- 408 the solubility and permeability of the diuretic drug furosemide via multicomponent crystal
- forms. Int J Pharm 587, 119694. https://doi.org/10.1016/j.ijpharm.2020.119694
- 410 El-Awady, R., Saleh, E., Hashim, A., Soliman, N., Dallah, A., Elrasheed, A., Elakraa, G., 2017.
- The Role of Eukaryotic and Prokaryotic ABC Transporter Family in Failure of
- Chemotherapy. Front Pharmacol 7. https://doi.org/10.3389/fphar.2016.00535
- Gangireddy, M.S.R., Badavath, V.N., Velez, C., Loeanurit, N., Thakur, A., Maddipati, V.C.,
- Katari, N.K., Acevedo, O., Boonyasuppayakorn, S., Gundla, R., 2022. Discovery of 3-
- chlorobenzyl-linked 1,9-diazaspiro[5.5]undecane derivatives, a lead for dengue virus type
- 416 2 infection. New Journal of Chemistry 46, 1087–1098.
- 417 https://doi.org/10.1039/D1NJ02453A
- Genheden, S., Ryde, U., 2015. The MM/PBSA and MM/GBSA methods to estimate ligand-
- 419 binding affinities. Expert Opin Drug Discov 10, 449–461.
- 420 https://doi.org/10.1517/17460441.2015.1032936
- Ghadi, R., Dand, N., 2017. BCS class IV drugs: Highly notorious candidates for formulation
- development. Journal of Controlled Release.
- 423 https://doi.org/10.1016/j.jconrel.2017.01.014
- 424 Hao, X., Li, J., Wang, C., Zhao, X., He, X., Sun, C.C., 2022. Profoundly improved
- photostability of dimetronidazole by cocrystallization. CrystEngComm 24, 6165–6171.
- 426 https://doi.org/10.1039/D2CE00597B

- Jorgensen, W.L., Chandrasekhar, J., Madura, J.D., Impey, R.W., Klein, M.L., 1983.
- Comparison of simple potential functions for simulating liquid water. J Chem Phys 79,
- 429 926–935. https://doi.org/10.1063/1.445869
- 430 Kataoka, M., Yonehara, A., Minami, K., Takagi, T., Yamashita, S., 2023. Control of
- Dissolution and Supersaturation/Precipitation of Poorly Water-Soluble Drugs from
- Cocrystals Based on Solubility Products: A Case Study with a Ketoconazole Cocrystal.
- 433 Mol Pharm 20, 4100–4107. https://doi.org/10.1021/acs.molpharmaceut.3c00237
- Kavanagh, O.N., Wang, C., Walker, G.M., Sun, C.C., 2021. Modulation of the powder
- properties of lamotrigine by crystal forms. Int J Pharm 595, 120274
- 436 https://doi.org/10.1016/j.ijpharm.2021.120274
- Kumari, N., Bhattacharya, B., Roy, P., Michalchuk, A.A.L., Emmerling, F., Ghosh, A., 2019.
- Enhancing the Pharmaceutical Properties of Pirfenidone by Mechanochemical
- Cocrystallization. Cryst Growth Des 19, 6482–6492.
- 440 https://doi.org/10.1021/acs.cgd.9b00932
- 441 Kumari, N., Ghosh, A., 2020. Cocrystallization: Cutting Edge Tool for Physicochemical
- Modulation of Active Pharmaceutical Ingredients. Curr Pharm Des 26, 4858–4882.
- https://doi.org/10.2174/1381612826666200720114638
- Kumari, N., Roy, P., Roy, S., Parmar, P., Chakraborty, S., Das, S., Pandey, N., Bose, A.,
- Bansal, A., Ghosh, A., n.d. Investigating the Role of the Reduced Solubility of the
- Pirfenidone–Fumaric Acid Cocrystal in Sustaining the Release Rate from Its Tablet
- Dosage Form by Conducting Comparative Bioavailability Study in Healthy Human
- Volunteers. Mol Pharm 0, null-null. https://doi.org/10.1021/acs.molpharmaceut.2c00052
- Kundu, S., Kumari, N., Soni, S.R., Ranjan, S., Kumar, R., Sharon, A., Ghosh, A., 2018.
- Enhanced Solubility of Telmisartan Phthalic Acid Cocrystals within the pH Range of a
- 451 Systemic Absorption Site. ACS Omega 3, 15380–15388.
- 452 https://doi.org/10.1021/acsomega.8b02144
- 453 Li, L., Pang, Z., Ma, K., Gao, Y., Zheng, D., Wei, Y., Zhang, J., Qian, S., 2021. Effect of
- 454 Coformer Selection on In Vitro and In Vivo Performance of Adefovir Dipivoxil
- 455 Cocrystals. Pharm Res 38, 1777–1791. https://doi.org/10.1007/s11095-021-03116-7
- 456 Maier, J.A., Martinez, C., Kasavajhala, K., Wickstrom, L., Hauser, K.E., Simmerling, C., 2015.
- 457 ff14SB: Improving the Accuracy of Protein Side Chain and Backbone Parameters from
- 458 ff99SB. J Chem Theory Comput 11, 3696–3713. https://doi.org/10.1021/acs.jctc.5b00255
- Manin, A.N., Drozd, K. V., Surov, A.O., Churakov, A. V., Volkova, T. V., Perlovich, G.L.,
- 460 2020. Identification of a previously unreported co-crystal form of acetazolamide: a
- 461 combination of multiple experimental and virtual screening methods. Physical Chemistry
- 462 Chemical Physics 22, 20867–20879. https://doi.org/10.1039/D0CP02700F
- Mannava, M.K.C., Garai, A., Nangia, A.K., 2023. Diffusion and Flux Improvement of Drugs
- 464 through Complexation. Mol Pharm 20, 2293–2316.
- https://doi.org/10.1021/acs.molpharmaceut.3c00159

- 466 Mannava, M.K.C., Gunnam, A., Lodagekar, A., Shastri, N.R., Nangia, A.K., Solomon, K.A.,
- 2021. Enhanced solubility, permeability, and tabletability of nicorandil by salt and
- 468 cocrystal formation. CrystEngComm 23, 227–237. https://doi.org/10.1039/d0ce01316a
- 469 Meng, S.-S., Yu, Y.-M., Bu, F.-Z., Yan, C.-W., Wu, Z.-Y., Li, Y.-T., 2023. Cocrystallization-
- Driven Double-Optimized Stratagem toward Directional Self-Assembly for the First
- 471 Ternary Salt Cocrystal of Cardiotonic Drug Milrinone with Different Phenolic Acids
- Exhibits Optimal In Vitro / Vivo Biopharmaceutical Peculiarities. Mol Pharm.
- https://doi.org/10.1021/acs.molpharmaceut.3c00230
- 474 Mohd Siddique, M.U., Thakur, A., Shilkar, D., Yasmin, S., Halakova, D., Kovacikova, L.,
- Prnova, M.S., Stefek, M., Acevedo, O., Dasararaju, G., Devadasan, V., Mondal, S.K.,
- Jayaprakash, V., 2021. Non-carboxylic acid inhibitors of aldose reductase based on N-
- substituted thiazolidinedione derivatives. Eur J Med Chem 223, 113630.
- 478 https://doi.org/10.1016/j.ejmech.2021.113630
- 479 Morris, G.M., Huey, R., Lindstrom, W., Sanner, M.F., Belew, R.K., Goodsell, D.S., Olson,
- 480 A.J., 2009. AutoDock4 and AutoDockTools4: Automated docking with selective receptor
- 481 flexibility. J Comput Chem 30, 2785–2791. https://doi.org/10.1002/jcc.21256
- 482 Morris, G.M., Huey, R., Olson, A.J., 2008. Using AutoDock for Ligand-Receptor Docking.
- 483 Curr Protoc Bioinformatics 24. https://doi.org/10.1002/0471250953.bi0814s24
- Nath, C., Badavath, V.N., Thakur, A., Ucar, G., Acevedo, O., Mohd Siddique, M.U.,
- Jayaprakash, V., 2018. Curcumin-based pyrazoline analogues as selective inhibitors of
- human monoamine oxidase A. Medchemcomm 9, 1164–1171.
- 487 https://doi.org/10.1039/C8MD00196K
- 488 Ng, S.-F., Rouse, J., Sanderson, D., Eccleston, G., 2010. A Comparative Study of
- 489 Transmembrane Diffusion and Permeation of Ibuprofen across Synthetic Membranes
- 490 Using Franz Diffusion Cells. Pharmaceutics 2, 209–223.
- https://doi.org/10.3390/pharmaceutics2020209
- 492 Palanisamy, V., Sanphui, P., Jyothi, V.G.S.S., Shastri, N.R., Bolla, G., Palanisamy, K.,
- 493 Prakash, M., Vangala, V.R., 2021. Tuning Diffusion Permeability of an Anti-Retroviral
- Drug, Emtricitabine, via Multicomponent Crystallizations. Cryst Growth Des 21, 1548–
- 495 1561. https://doi.org/10.1021/acs.cgd.0c01344
- 496 Pandey, N., Ghosh, A., 2022. An outlook on permeability escalation through cocrystallization
- for developing pharmaceuticals with improved biopharmaceutical properties. J Drug
- 498 Deliv Sci Technol 76. https://doi.org/10.1016/j.jddst.2022.103757
- 499 Price, O.M., Thakur, A., Ortolano, A., Towne, A., Velez, C., Acevedo, O., Hevel, J.M., 2021.
- Naturally occurring cancer-associated mutations disrupt oligomerization and activity of
- protein arginine methyltransferase 1 (PRMT1). Journal of Biological Chemistry 297,
- 502 101336. https://doi.org/10.1016/j.jbc.2021.101336
- Roe, D.R., Cheatham, T.E., 2018. Parallelization of CPPTRAJ enables large scale analysis of
- molecular dynamics trajectory data. J Comput Chem 39, 2110–2117.
- 505 https://doi.org/10.1002/jcc.25382

- Roy, P., Ghosh, A., 2020a. Progress on cocrystallization of poorly soluble NME's in the last decade. CrystEngComm 22, 6958–6974. https://doi.org/10.1039/D0CE01276A
- Roy, P., Ghosh, A., 2020b. Mechanochemical cocrystallization to improve the physicochemical properties of chlorzoxazone. CrystEngComm 22, 4611–4620. https://doi.org/10.1039/D0CE00635A
- 511 Roy, P., Pandey, N., Kumari, N., Baidya, R., Mary, Y.S., Mary, Y.S., Ghosh, A., 2022.
- Development of sulfamethoxazole-succinimide cocrystal by mechanochemical
- 513 cocrystallization An insight into spectroscopic, electronic, chemical conformation and
- physicochemical properties. Chemical Engineering Research and Design 185.
- 515 https://doi.org/10.1016/j.cherd.2022.07.012
- Sanphui, P., Devi, V.K., Clara, D., Malviya, N., Ganguly, S., Desiraju, G.R., 2015. Cocrystals
- of Hydrochlorothiazide: Solubility and Diffusion/Permeability Enhancements through
- 518 Drug-Coformer Interactions. Mol Pharm 12, 1615–1622.
- 519 https://doi.org/10.1021/acs.molpharmaceut.5b00020
- Seelig, A., 2020. P-Glycoprotein: One Mechanism, Many Tasks and the Consequences for Pharmacotherapy of Cancers. Front Oncol 10. https://doi.org/10.3389/fonc.2020.576559
- Seo, J.-W., Hwang, K.-M., Lee, S.-H., Kim, D.-W., Park, E.-S., 2018. Preparation and
- 523 characterization of adefovir dipivoxil-stearic acid cocrystal with enhanced
- physicochemical properties. Pharm Dev Technol 23, 890–899.
- 525 https://doi.org/10.1080/10837450.2017.1334664
- 526 Shaikh, F., Bhakat, S., Thakur, A., Radadia, A., Soliman, M.E.S., Shah, A., 2015. Identification
- of Novel GSK1070916 Analogs as Potential Aurora B Inhibi-tors: Insights from
- Molecular Dynamics and MM/GBSA Based Rescoring, Letters in Drug Design &
- 529 Discovery.
- Shajan, D.K., Pandey, N., Ghosh, A., Chanduluru, H.K., Sanphui, P., 2023. Investigating the
- Effect of Emtricitabine Cocrystals with Aromatic Carboxylic Acids on Solubility and
- Diffusion Permeability. Cryst Growth Des. https://doi.org/10.1021/acs.cgd.3c00485
- 533 Shinozaki, T., Ono, M., Higashi, K., Moribe, K., 2019. A Novel Drug-Drug Cocrystal of
- Levofloxacin and Metacetamol: Reduced Hygroscopicity and Improved Photostability of
- 535 Levofloxacin. J Pharm Sci 108, 2383–2390. https://doi.org/10.1016/j.xphs.2019.02.014
- Sugandha, K., Kaity, S., Mukherjee, S., Isaac, J., Ghosh, A., 2014. Solubility Enhancement of
- Ezetimibe by a Cocrystal Engineering Technique. Cryst Growth Des 14, 4475–4486.
- 538 https://doi.org/10.1021/cg500560w
- Sun, C.C., 2013. Cocrystallization for successful drug delivery. Expert Opin Drug Deliv 10,
 201–213. https://doi.org/10.1517/17425247.2013.747508
- Sun, C.C., Hou, H., 2008. Improving Mechanical Properties of Caffeine and Methyl Gallate
- 542 Crystals by Cocrystallization. Cryst Growth Des 8, 1575–1579.
- 543 https://doi.org/10.1021/cg700843s
- Suzuki, Y., Muangnoi, C., Thaweesest, W., Teerawonganan, P., Ratnatilaka Na Bhuket, P.,
- Titapiwatanakun, V., Yoshimura-Fujii, M., Sritularak, B., Likhitwitayawuid, K.,

- Rojsitthisak, P., Fukami, T., 2019. Exploring Novel Cocrystalline Forms of
- Oxyresveratrol to Enhance Aqueous Solubility and Permeability across a Cell Monolayer.
- 548 Biol Pharm Bull 42, 1004–1012. https://doi.org/10.1248/bpb.b19-00048
- Tanaka, R., Hattori, Y., Otsuka, M., Ashizawa, K., 2020. Application of spray freeze drying to
- theophylline-oxalic acid cocrystal engineering for inhaled dry powder technology. Drug
- Dev Ind Pharm 46, 179–187. https://doi.org/10.1080/03639045.2020.1716367
- Thakur, A., Sharma, G., Badavath, V.N., Jayaprakash, V., Merz, K.M., Blum, G., Acevedo,
- O., 2022. Primer for Designing Main Protease (M pro) Inhibitors of SARS-CoV-2. J Phys
- Chem Lett 13, 5776–5786. https://doi.org/10.1021/acs.jpclett.2c01193
- 555 U.S. Department of Health and Human Services, Food and Drug Administration, Center for
- Drug Evaluation and Research (CDER), 2008. Regulatory Classification of
- Pharmaceutical Co-Crystals Guidance for Industry [WWW Document]. FDA. URL
- https://www.fda.gov/files/drugs/published/Regulatory-Classification-of-Pharmaceutical-
- 559 Co-Crystals.pdf (accessed 1.8.22).
- Vangala, V.R., Chow, P.S., Tan, R.B.H., 2012. Co-Crystals and Co-Crystal Hydrates of the
- Antibiotic Nitrofurantoin: Structural Studies and Physicochemical Properties. Cryst
- Growth Des 12, 5925–5938. https://doi.org/10.1021/cg300887p
- Varma, M.V.S., Sateesh, K., Panchagnula, R., 2005. Functional Role of P-Glycoprotein in
- Limiting Intestinal Absorption of Drugs: Contribution of Passive Permeability to P-
- Glycoprotein Mediated Efflux Transport. Mol Pharm 2, 12–21.
- 566 https://doi.org/10.1021/mp0499196
- Vassetti, D., Pagliai, M., Procacci, P., 2019. Assessment of GAFF2 and OPLS-AA General
- Force Fields in Combination with the Water Models TIP3P, SPCE, and OPC3 for the
- Solvation Free Energy of Druglike Organic Molecules. J Chem Theory Comput 15, 1983–
- 570 1995. https://doi.org/10.1021/acs.jctc.8b01039
- 571 Wang, E., Sun, H., Wang, J., Wang, Z., Liu, H., Zhang, J.Z.H., Hou, T., 2019. End-Point
- Binding Free Energy Calculation with MM/PBSA and MM/GBSA: Strategies and
- 573 Applications in Drug Design. Chem Rev 119, 9478–9508.
- 574 https://doi.org/10.1021/acs.chemrev.9b00055
- Wang, J., Dai, X.L., Lu, T.B., Chen, J.M., 2021. Temozolomide-Hesperetin Drug-Drug
- 576 Cocrystal with Optimized Performance in Stability, Dissolution, and Tabletability. Cryst
- Growth Des 21, 838–846. https://doi.org/10.1021/acs.cgd.0c01153
- Wang, K., Hao, Y., Wang, C., Zhao, X., He, X., Sun, C.C., 2022. Simultaneous improvement
- of physical stability, dissolution, bioavailability, and antithrombus efficacy of Aspirin and
- Ligustrazine through cocrystallization. Int J Pharm 616, 121541.
- 581 https://doi.org/10.1016/j.ijpharm.2022.121541
- 582 Wang, X., Wang, L., Yao, C., Xie, G., Song, S., Li, H., Qu, Y., Tao, X., 2021. Novel
- Formulations of the Antiviral Drug Favipiravir: Improving Permeability and Tabletability.
- Cryst Growth Des 21, 3807–3817. https://doi.org/10.1021/acs.cgd.1c00150

Zhou, Z., Li, W., Sun, W.-J., Lu, T., Tong, H.H.Y., Sun, C.C., Zheng, Y., 2016.
Resveratrol cocrystals with enhanced solubility and tabletability. Int J Pharm 509,
391–399. https://doi.org/10.1016/j.ijpharm.2016.06.006